Dergi Listesi

Dergi Adı
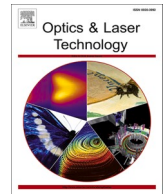
ISSN 0030-3992

Yıl 2021

[Temizle] [Ara]

No	Yıl	Dergi Adı	ISSN	Çeyreklik Grup	Katsayı	kategori	Dergi Puanı
100714	2021	OPTICS AND LASER TECHNOLOGY	0030-3992	Q1	1	SCIE	

Sayfada 10 ∨ Kayıt Göster

Önceki

1 Kayıttan 1 - 1 Arası Kayıtlar

Systematic optical study of high-x InxGa1-xAs/InP structures for infrared photodetector applications

Smiri Badreddine [a,b,*], R.S. Joshya [a], Demir Ilkay [c], Saidi Faouzi [b], Altuntas Ismail [c], Delphine Lagarde [a], Cedric Rober [a], Marie Xavier [a], Maaref Hassen [b]

[a] Université de Toulouse, INSA-CNRS-UPS, LPCNO, Toulouse, France
[b] Université de Monastir, Laboratoire de Micro-Optoélectronique et Nanostructures (LR99ES29), Faculté des Sciences, 5019 Monastir, Tunisia
[c] Department of Nanotechnology Engineering and Nanophotonics Research and Application Center, Sivas Cumhuriyet University, 58140 Sivas, Turkey

ABSTRACT

Optical and structural properties in high-x In$_x$Ga$_{1-x}$As (x > 0.65) samples with varying indium concentration grown on InP (1 0 0) substrate are reported. By increasing the indium fraction, it was found by the high-resolution X-ray diffraction (HR-XRD) study that the dislocation density in the In$_x$Ga$_{1-x}$As epitaxial layer significantly increased, and the surface quality deteriorated remarkably. Photoreflectance (PR) spectra show the presence of Franz-Keldysh Oscillations (FKOs) features above the In$_x$Ga$_{1-x}$As energy bandgap. The strain-induced electric field is then estimated directly from the FKOs periods. Temperature-dependent photoluminescence (TDPL) measurements from 10 K to 300 K showed carrier locations (S-shape). This abnormal behavior is due to the dislocation density associated with fluctuations in the indium concentration. A quasi-stationary rate equation model for the temperature-dependent luminescence spectra of the localized state material system is proposed to interpret the band gap emission process quantitatively. Low-temperature (10 K) time-resolved PL measurements show the increase of lifetime with increasing the indium concentration. Yet, the addition of only 1.7% of indium concentration results in a strong enhancement of PL lifetime by ~ 80%.

All these results reveal a more precise picture of the localization and recombination mechanisms of photo-generated carriers in the InGaAs layer, which could be the crucial factors in controlling the performance of high indium content InGaAs SWIR detector.

1. Introduction

High-x (x > 0.53) In$_x$Ga$_{1-x}$As/InP material systems have achieved great success in optoelectronics and received enormous research interest. One of the most important applications is short-wave (1–3.6 um) infrared (SWIR) detectors [1,2], which is required for the various field, such as spectroscopy [3], astronomy [4] and medicine [5]. Yet, in order to extend the response of the detector to longer wavelengths, it is necessary to grow the In$_x$Ga$_{1-x}$As alloy with a high In content (x > 0.53) [6]. Epitaxial growth requires suitable substrate materials, but lattice mismatch always limits the heteroepitaxy of such materials.

However, the composition of the In$_x$Ga$_{1-x}$As layer is very important because it affects the electronic properties of these devices. In order to achieve this goal, the × value in In$_x$Ga$_{1-x}$As must be increased to 0.65 to

0.85, which will cause a significant lattice mismatch (+0.55% to + 2.2%) between the In$_x$Ga$_{1-x}$As layer and the InP substrate [1]. The growth of high-x In is accompanied by the generation of dislocations and other defects caused by lattice mismatch, which will lead to poor surface quality and no uniformity in the alloy composition [7,8]. For the reasons mentioned above, carriers are captured and redistributed by spatial potential fluctuation and localized energy states, which is referred to as carrier location [9,10]. Moreover, carrier's localization in semiconductor systems has been extensively studied [11]. Such carrier localization phenomenon usually increases the dark current of the devices [12]. In this framework, Xiaoli et al. [6] have shown that this high dark current is still one of the critical technology issues for the development of extended-wavelength In$_x$Ga$_{1-x}$As/InP (x > 0.53) photodetectors (PDs).

The influence of carrier localization is also manifested in the temperature abnormality « S-shape » of the peak PL energy and the form of the low-temperature PL decay curve[13,14]. In order to fit the curve, several methods have been used, such as double exponential model, triple exponential model, stretched model, etc [15-17]. Nevertheless, these methods only provide mathematical fitting without detailed physical explanation. Hence, the exact nature of the carrier localization and carrier dynamics are key issues for understanding and improving InGaAs devices. This type of high $\times$ In$_x$Ga$_{1-x}$As anomalous behavior requires a thorough study to fully explain the physics behind this phenomenon, especially the dark current mechanism. Furthermore, more research is required on both device structure and dark current mechanism of InGaAs photodetectors.

In this letter, we used a luminescence model for localized state ensemble (LSE) developed by Li et al. [16], taking into account generation, thermal activation, and recapturing of excitons by using Pässler model to follow the energy evolution. Moreover, we used the photoreflectance (PR) spectroscopy to obtain important properties of the samples. By analyzing the Franz–Keldysh oscillations, we estimated the built-in electric fields. In addition, time-resolved PL measurements (TRPL) were carried out at 10 K. The investigation of the electronic properties presented in this paper could yield on improvement of the efficiency of the high-x In$_x$Ga$_{1-x}$As/InP structures (x > 0.65) and make them useful for many types of devices used in optoelectronics and microelectronics.

2. Experimental details

The three samples, 190 nm-thick In$_x$Ga$_{1-x}$As investigated in this paper, were fabricated by Metalorganic Vapor Phase Epitaxy (MOVPE) at 560 °C on InP (1 0 0) substrate. For the In$_x$Ga$_{1-x}$As samples called S1, S2 and S3, it corresponds to $\times$ = 0.650, x = 0.661 and $\times$ = 0.667 and are described in detail in Ref [7].

The samples were characterized by HR-XRD, PR, PL and TRPL spectroscopy. Then, the samples were characterized by HR-XRD and PL. The HR-XRD measurements were performed using Rigaku SmartLab diffractometer, equipped with a rotating Cu anode (wavelength Kα = 1.54056 A) which provides 9 kW X-ray power and four bounced Ge (2 2 0) monochromator allowing a 2theta precision of 0.0004°. We used a tungsten lamp in PR, and the modulating source an Ar$^+$ laser (532 nm) chopped at 250 Hz. An InGaAs photodiode detected the PR signal. With PL spectroscopy, we studied the samples between 10 and 300 K while keeping the samples in a closed-cycle helium circulation cryostat. The samples are excited using 514.5 nm line of the continuous-wave Ar$^+$ laser. The excitation density was fixed at 80 W/cm^2. The luminescence was dispersed using a JOBIN YVON HRD1 monochromator and detected by a cooled Ge diode detector with a built-in amplifier. The TRPL spectra were measured at a temperature of 8 K using a closed cycle cryostat. In this case, the PL dynamics was excited by a frequency-doubled Ti: Sa laser at λ$_{exc}$ = 375 nm, the laser-pulse duration was 2 ps pulse-repetition frequency was 4 MHz. A super conducting nanowire single photon detector (single quantum) detected the PL signal from the InGaAs samples using a time-correlated single-photon counting system (picottarp from picoquant). The instrument response function is at the order 150 ps. The excitation power is 50 mW, and the laser spot size is about 10 μm^2).

3. Results and discussions

3.1. HR-XRD results

Fig. 1 shows the HR-XRD patterns of In$_x$Ga$_{1-x}$As epilayer on InP substrate for different indium concentrations. The peaks at 63.5° and 62.2° corresponds to InP and In$_x$Ga$_{1-x}$As respectively. Increase of indium content in In$_x$Ga$_{1-x}$As epilayer shows a decrease in angle due to the increase of lattice constant [7]. The FWHM of an epilayer examined by HR-XRD is an important parameter to characterize the crystalline
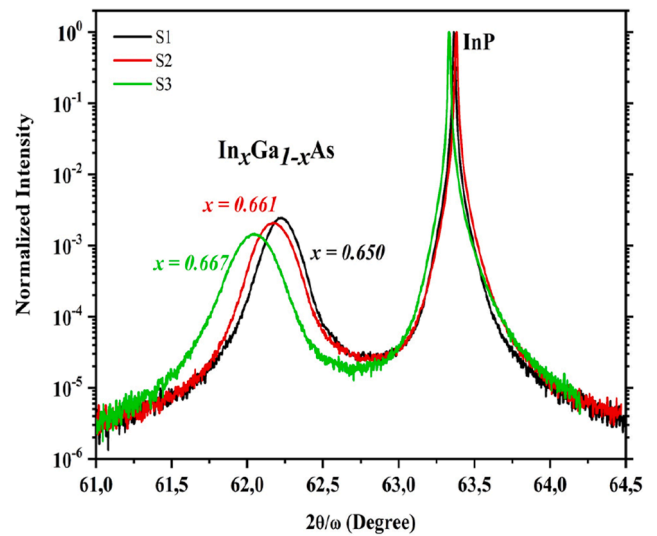

Fig. 1. 2θ/ω HR-XRD spectra of the In$_x$Ga$_{1-x}$As layers having different In alloys grown on InP by MOVPE [7].

quality and dislocation. The values of lattice parameter and dislocation density are calculated and summarized in the Table 1. Increase of indium content from $\times$ = 0.650 to 0.667 shows an increase of the dislocation density from 2.1*10^9 m^{-2} to 3.1*10^9 cm^{-2}. However, these values only reflect the average dislocation density of the epilayer. The lattice mismatch has also been determined for different indium content in In$_x$Ga$_{1-x}$As/InP. The addition of indium increases the lattice mismatch, but this is significantly less compared to GaAs substrate [18,19].

3.2. Photoreflectance results

The photoreflectance technique (PR) is an important and useful tool to investigate and qualify the interband transitions and electric field distributions in semiconductor and multilayer structures because of its derivatives-like nature and sharp spectral features. The main advantage of PR is its high sensitivity, even at room temperature. However, the existence of overlapping spectral characteristics of different regions of multilayer structures can complicate PR analysis.

Fig. 2 shows the PR spectra of the three high-x In$_x$Ga$_{1-x}$As samples at room temperature. PR is a differential form of reflectance; therefore, its sensitivity is very high, as shown in Fig. 2. In this case, transitions originating from the InP substrate and InGaAs layer are visible [20,21]. In addition, the PR spectra reveal many oscillations above the high-x In$_x$Ga$_{1-x}$As layer and InP substrate for the three samples [22,23]. These oscillations are related to the Franz-Keldysh oscillations (FKO), resulting from an electric field present in the different samples. FKO has a regular periodicity and presents only the energies above the critical point [24]. There appear to be two sets of FKOs, one related to the InP gamma-point of 1.39 (±0.02) eV and the other linked with the InGaAs bandgap. Note that the shape and position of the PR spectrum in all samples are not identical. The shift in the extrema of the FKOs is observed. This is due to the variation of lattice mismatch between the InGaAs layer and the InP substrate, increasing the indium content in

Table 1
In$_x$Ga$_{1-x}$As samples characteristics and calculated parameters using HR-XRD.

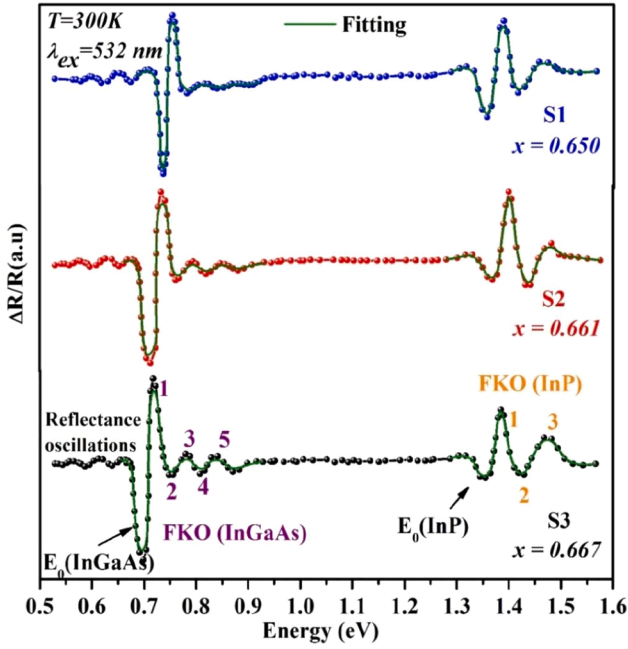| Samples	Indium (x =)	Lattice parameter ($A°$)	Dislocation density ($10^9 cm^{-2}$) [7]	Lattice mismatch (%)
S1	0.650	5.9545	2.1	1.44
S2	0.661	5.9592	2.6	1.54
S3	0.667	5.9618	3.1	1.58

Fig. 2. Room temperature PR spectra (dots) obtained from samples S1, S2 and S3 at different indium concentration and fits (green lines) performed using Eq. ~ 1.

In$_x$Ga$_{1-x}$As. The FKOs have been frequently used to define the built-in electric field inside the semiconductor device. In this article, we will only be interested in this FKO related to the InGaAs layer.

Now, to estimate the value of electric fields in the high-x In$_x$Ga$_{1-x}$As layer, the FKO period is analyzed using an asymptotic expression for the PR line shape given by Aspnes and Studna [25]. In the region 0.7–0.9 eV, the oscillatory $\Delta R/R$ signal can be described by:

$$\frac{\Delta R}{R} = \frac{1}{E^2(E-E_0)}\exp\left[-2(E-E_0)^{\frac{1}{2}}\frac{\Gamma}{(h\Omega)^{\frac{3}{2}}}\right]\cos\left[\frac{4}{3}\left(\frac{E-E_0}{h\Omega}\right)^{\frac{3}{2}}+\varnothing\right] \quad (1)$$

where Γ is the broadening parameter, É is an arbitrary phase factor and $h\Omega$ is the electro-optic energy expressed as follows:

$$h\Omega = \left(\frac{q^2 h^2 Fint^2}{8\mu}\right)^{1/3} \quad (2)$$

Note that q is the electron charge, μ is the reduced inter-band effective mass in the electric field direction and Fint is the internal electric field.

In order to extract PR parameters (Fint, $\hbar\Omega$, etc.), the energy of FKO extrema (E$_n$) is given by [26]:

$$E_n = (h\Omega)H_n + E_0 \quad (3)$$

and

$$H_n = \left[\left(\frac{3\Pi}{2}\right)(n-1/2)\right]^{2/3} \quad (4)$$

Thus, by plotting E_n as a function of H_n (see Fig. 3), from linear fitting, we can determine $\hbar\Omega$ and E$_0$ from the slope and the intersection with the ordinate at the origin, respectively. Recalling equation (2), F$_{int}$ can be extracted by:

$$F_{int} = \sqrt{\frac{2\mu(h\Omega)^3}{q^2 h^2}} \quad (5)$$

A summary of the experimental results is shown in Table 2. The obtained values of E$_0$ are 0.73, 0.71 and 0.67 eV for sample S1, S2 and S3, respectively. InGaAs band gap value is close to that obtained by
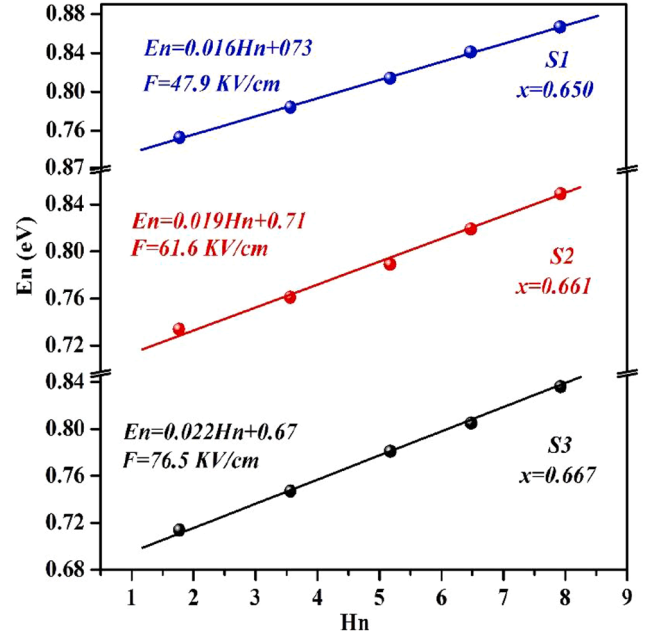

Fig. 3. Plot of the energy extremes E$_n$ vs. index number H$_n$ for each sample. The straight lines are fittings to the FKO model using eq.3. The lines slope and ordinates to origin relate to the electric field strength F$_{int}$ and the InGaAs bandgap energy E0.

Table 2
Summary of PR results for In$_x$Ga$_{1-x}$As layers. Bandgap energy E$_0$, broadening Γ, internal electric field F$_{int}$, and electro-optical energy hΩ. Some value from the literature are added.

Sample	x$_{In}$	E$_0$ (eV)	Γ (meV)	hΩ (meV)	F$_{int}$ (kV/cm)	
					Exp	Ref.
S1	0.650	0.73 ± 0.02	3.2 ± 0.1	16 ± 1	47.9 ± 0.2	F = 155 ± 5 (x$_{In}$ = 0.15) [28]
S2	0.661	0.71 ± 0.02	4.9 ± 0.1	19 ± 1	61.6 ± 0.2	F = 30 ± 2 (x$_{In}$ = 0.53) [27]
S3	0.667	0.67 ± 0.02	5.1 ± 0.1	22 ± 1	76.5 ± 0.2	F = 50 (x$_{In}$ = 0.65) [29]

HR_XRD measurements. To evaluate Γ for the InGaAs transitions, experimental linewidths are least-squares fits equation (1) as shown in Fig. 2. It is interesting to note that the values Γ increase with increasing indium concentration in In$_x$Ga$_{1-x}$As. However, we can see significant differences in the internal electric field strength in the samples. It is important to note that sample S3 with the highest residual strain presents the highest internal electric field of 76.5 kV/m. According to D. Yan et al. [27], the value of the internal electric field in the ternary alloy semiconductor (In$_{0.53}$Ga$_{0.47}$As), lattice-matched to InP substrate is 30 kV/cm. Yet, for the sample S1, S2 and S3, the residual strain in epitaxial layers increases with the increase of indium concentration. As all the structures examined in this paper have the same geometric structure, we believe that the significant difference in the electric fields is due to different amounts of dislocation density. A high concentration of dislocation density will reduce the quality of the structure, form electron dispersion centers, and generate a strong built-in electric field in the sample.

3.3. Photoluminescence results

Fig. 4 compares the PL spectra of the In$_x$Ga$_{1-x}$As epilayer with various indium concentrations (x = 0.650, 0.661, 0.667) at 10 K under the same excitation power density of 80 W/cm^2 of 514 nm. As indium
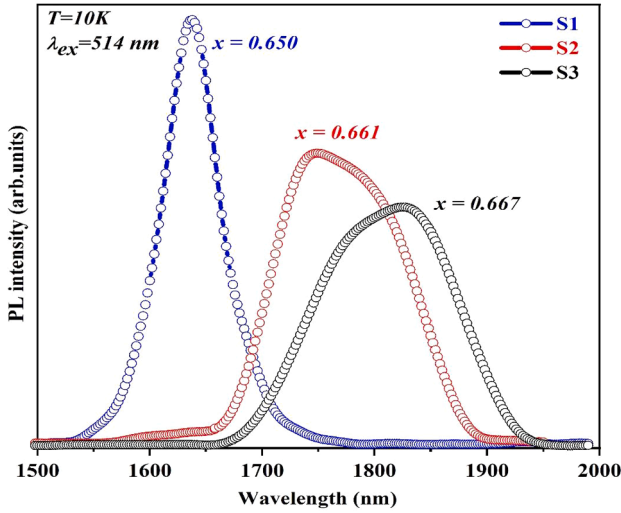
Fig. 4. Comparison of the PL spectra of the three InGaAs samples with different In concentrations at 10 K.

concentration increases to a small amount of 1.7%, the PL peak shows a large red-shift of about 170 nm, which is most suitable for short-wave infrared applications. The FWHM of the PL emission increases significantly with increasing indium concentration in $In_xGa_{1-x}As$: incorporating high indium in $In_xGa_{1-x}As$ induces the structural inhomogeneities that cause localized potential fluctuations in its band structure [30,31]. Also, as shown in Fig. 5, the PL peak energy as a function of lattice temperature shows a "S-shape" (red/blue/red-shift) behavior which is the foot-print of the presence of localized carriers [7]. The S-shape behavior becomes more pronounced at high indium concentration. The phenomenon of the S-shape behavior at low temperature can be explained as follows : at cryogenic 10 K (*party I in* Fig. 6) the
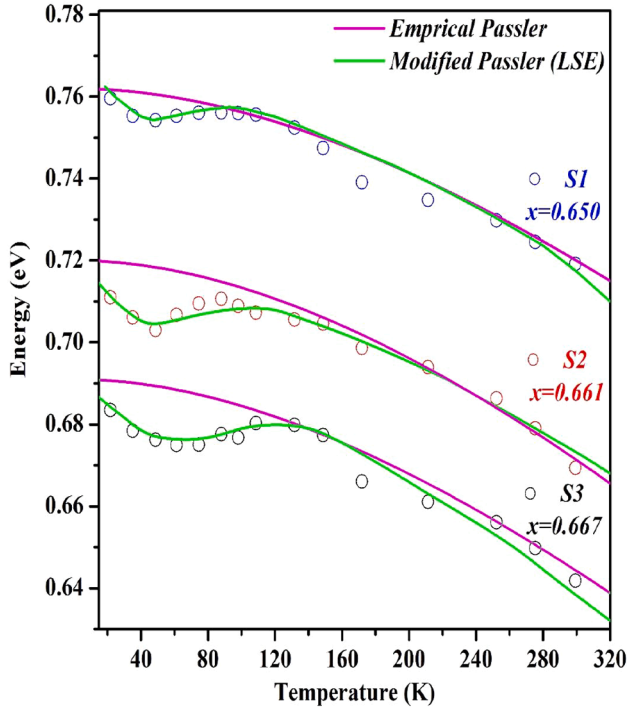

Fig. 5. The PL peak energy of $In_xGa_{1-x}As$ epilayer as a function of lattice temperature. green and red solid lines de- scribes the classical and modified Pässler model fit to the experimental data respectively. The parameters yielding to the best fit are tabulated in Table 3.
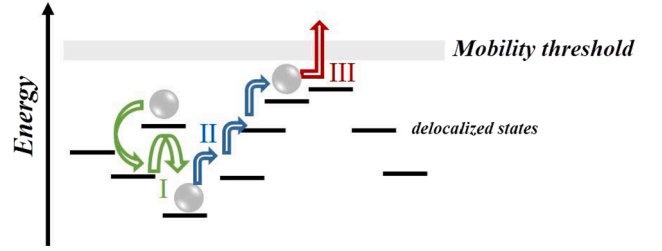

Fig. 6. Schematic diagram for describing the hopping of carriers in localized levels. Dotted lines I , II and III indicate the transition process of carriers between different localization states with increasing temperatures.

excitons are strongly located in levels whose energy distribution extends within the band gap of the material. As lattice temperature to $\sim$ 60 K, excitons thermalize and relax to the local minima (alloy disorder) so that the PL peak energy decreases and we observed the first red shift. With further increase of temperature from 60 K to 100 K (*party II in* Fig. 6), the localized carriers gain enough thermal energy to be transferred to higher energy levels in the band-tails until they reaches maximum of band continuum, thus leading to blue-shift of the PL peak energy. Finally, when the lattice temperature increased above 100 K (*party III in* Fig. 6), the carriers are thermally activated and prevented from localization (free carrier recombination). A schematic diagram is shown in Fig. 6. The classic models such as Varshni [15], Vina [16], and Pässler [17] explain well the behavior at high temperature but unable to reproduce it at low temperature. The localized effects at low temperature can be explained using the Localized State Exciton Model or modified Pässler model with the impact of thermal redistribution of localized carriers [32-34]:

$$E(T) = E(0) - \frac{\alpha\theta}{2}\left[\sqrt[p]{1 + \left(\frac{2T}{\theta}\right)} - 1\right] - x(T).K_B.T \qquad (6)$$

The second term describes the shrinking of band according to the classic Pässler equation with α and Θ are Varshni parameter and the Debye temperature, respectively. The dimensionless coefficient $\times$ (T) can be obtained by numerically solving the equation [35]:

$$xe^x = \left[1 + \left(\frac{\sigma}{K_B.T}\right)^2 - x\right]\left(\frac{\tau_r}{\tau_{tr}}\right)e^{\frac{E_0 - E_a}{K_B.T}} \qquad (7)$$

where σ is the broadening parameter for the distribution of the localized states at central energy E_0. τ_r, τ_{tr}, E_a and K_B are the radiative lifetime, non-radiative lifetime, activation energy, and the Boltzmann constant. At high temperature, the solution of equation (7) can be approximated to be:

$$x\left(\frac{\sigma}{K_B.T}\right)^2 \qquad (8)$$

Equation (6) can be rewritten as [10]:

$$(T) = E(0) - \frac{\alpha\theta}{2}\left[\sqrt[p]{1 + \left(\frac{2T}{\theta}\right)} - 1\right] - \frac{\sigma^2}{K_B.T} \qquad (9)$$

Fig. 5 shows compares the experimental data with the classical and modified Pässler Model. The modified Pässler model gives a good agreement with experimental data. The fitting parameters are summarized in Table 3.

Using the LSE model, the temperature dependence of the position of the PL peaks of the three S-shaped structures can be well reconstructed, as shown in Fig. 5. From the calculation, we obtained the same E_0 value as obtained by PR results. However, $\Delta E = E_a - E_0$ is a necessary parameter to understand the abnormal temperature dependence of temperature better. From a physical point of view, there are two situations. ΔE can be positive (+) or negative (-), but ΔE is usually positive. In our case, it is

Table 3
The best-fit parameters of the experimental data of $In_xGa_{1-x}As$ for different In content, obtained by the modified Pässler model.

Samples	x_{In}	E_0 (meV)	$Ea-E_0$(meV)	σ (meV)	τ_r/τ_{tr}	α (eV/k)	T (k)
S1	0.650	0.76	16.70	4.8	2000	2.70	200
S2	0.661	0.71	24.26	11.0	1500	2.73	185
S3	0.667	0.68	29.30	16.5	535	2.60	243

positive and it increases by increasing the indium concentration. For samples S3, S2, and S1, the values are 16.5 meV, 11.0 meV, and 4.8 meV, respectively, that is, E_a is located above E_0. In this case, the localized carriers are thermally activated to a higher energy state. This is why the S-shape is more evident in the S3 sample. This explains the larger occupied localized states and the proximity of empty states located at 10 K. In fact, the excitons gain enough thermal energy to overcome the small barrier and excite to a higher localized state above E_a with larger potential. The depth of potential fluctuation assigned by σ is the result of fluctuations in the indium composition and the presence of the electric field in our structures [31]. The potential depth is found to be 10.5; 15.0 and 16.8 meV. It is larger with increasing concentration indium and electric-filed. As a result, we can that the increase of potential depth increases the dark current of the devices, which could be the crucial factor in controlling the performance of high indium content $In_xGa_{1-x}As$ SWIR detector [36].

3.4. TRPL results

Time-resolved photoluminescence measurement was carried out to understand the influence of indium concentration on the carrier dynamics in the high-x $In_xGa_{1-x}As$ layers. The PL lifetime profile of $In_xGa_{1-x}As$ at 10 K for different indium concentrations are shown in Fig. 7. To obtain the PL lifetime, we fitted with a single-exponential decay, $I(t) = I_0*\exp(-\frac{t}{\tau})$ [37] where I_0 and τ are amplitude and decay time-constant, respectively. The lifetime is determined to be 0.33 ns, 0.49 ns, and 0.59 ns for the sample S1, S2, and S3, respectively [38]. Surprisingly, the low PL lifetime of 0.33 ns is obtained in sample S1, which has the best crystalline quality compared to the others. The addition of only 1.7% of indium concentration results in a strong enhancement of PL lifetime by ~ 80%. Regarding this increase of lifetime with increasing the indium concentration, two factors should be considered: the localization of
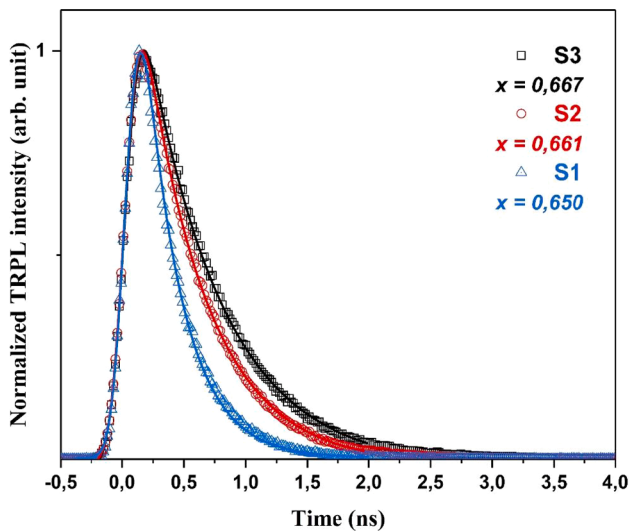
excitons and the local electric field. It is well known that the localization of excitons yields an increase in the radiation lifetime [39]. This could explain that the decay time in sample S3 is longer than the one in sample S1 as the excitons could be strongly localized. The larger electric-filed in the high-In structures could also lead to a spatial separation of electrons and holes, yielding an increase in recombination time [40].

Fig. 8 shows the measured PL lifetime τ_{InGaAs} vs. the pump power for an excitation wavelength of 375 nm. The PL lifetime of the $In_xGa_{1-x}As$ first increases and then saturates for pump powers beyond 60 μW. This could to due to the filling and saturation of localized states. Then of high density of carriers, the free excitons could be more sensitive to the local electric field, yielding an increase of the recombination time. This hypothesis should be confirmed by further investigations [41].

4. Conclusion

We have studied high-x $In_xGa_{1-x}As$ layers on InP substrates by HR-XRD, PL, PR and TRPL with varying indium concentration. PR measurement revealed oscillations above the InGaAs layer, which are related to the Franz-Keldysh oscillations (FKO). From an analysis of the FKO, we have estimated that the electric field increases with indium concentration. The temperature-dependent PL measurement demonstrates the critical role played by carrier localization. The S-shape behavior is the result of a competitive process between localized and non-localized carriers. For increasing indium concentration in InGaAs, the density of localization increases. Luminescence measurements have been successfully modeled and interpreted using the developed LSE model. These theoretical studies have quantitatively explained the temperature-dependent spectra observed. LT-TRPL measurements showed longer decay times in the high-x samples, which is likely due to increased localization and electric field effects.

Our works shows that the high defect densities leads the carrier's localization, thereby increasing the dark current of the device. In addition, it's imparts a deep level understanding of the behavior of carriers and optoelectronic parameters in high-x $In_xGa_{1-x}As$ structures. In the next work, we will study the compensation of the strain layer by adding the buffer layer in our high-x $In_xGa_{1-x}As$ structures for minimizing the dislocation density and the residual strain (ε) in the $In_xGa_{1-x}As$ epitaxial layer.

Declaration of Competing Interest

The authors declare that they have no known competing financial

Fig. 7. Normalized TRPL decay curves for $In_xGa_{1-x}As$/InP samples for x = 0.65 to 0.667 at 10 K with excitation power 50 μW. A single exponential decay (solid line) fitted with experimental data (symbols).
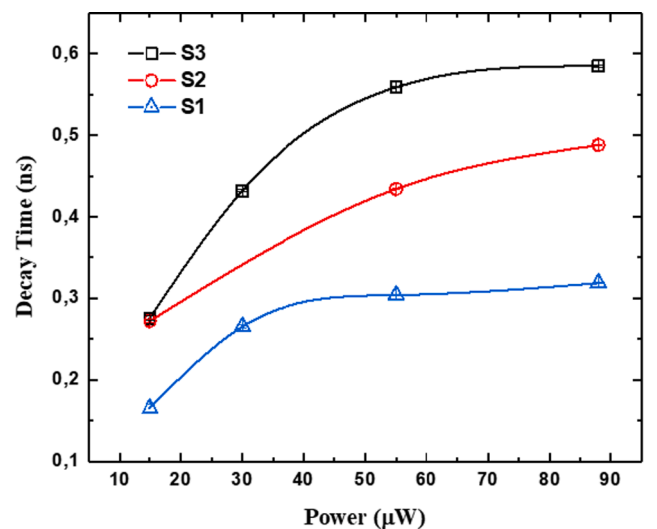
Fig. 8. PL lifetime as a function of excitation power (μW) of the $In_xGa_{1-x}As$/InP samples for x = 0.65 to 0.667 at 10 K.

interests or personal relationships that could have appeared to influence the work reported in this paper.

Acknowledgments

References

[1] P. Jurczak, K.A. Sablon, M. Gutiérrez, H. Liu, J. Wu, 2.5-μm InGaAs photodiodes grown on GaAs substrates by interfacial misfit array technique, Infrared Phys. Technol. 81 (2017) 320–324.

[2] J. Zhang, M. A. Itzler, H. Zbinden, et J.-W. Pan, « Advances in InGaAs/InP single-photon detector systems for quantum communication », *Light Sci. Appl.*, vol. 4, n° 5, Art. n° 5, mai 2015, doi: 10.1038/lsa.2015.59.

[3] I. Demir, I. Altuntas, B. Bulut, M. Ezzedini, Y. Ergun, S. Elagoz, Comprehensive growth and characterization study on highly n-doped InGaAs as a contact layer for quantum cascade laser applications, Semicond. Sci. Technol. 33 (5) (2018) 055005, https://doi.org/10.1088/1361-6641/aab9d3.

[4] C. L. Tan et H. Mohseni, « Emerging technologies for high performance infrared detectors », *Nanophotonics*, vol. 7, n° 1, p. 169–197, janv. 2018, doi: 10.1515/nanoph-2017-0061.

[5] X. Ji *et al.*, « Deep-level traps induced dark currents in extended wavelength In $_x$ Ga $_{1-x}$ As/InP photodetector », *J. Appl. Phys.*, vol. 114, n° 22, p. 224502, déc. 2013, doi: 10.1063/1.4838041.

[6] L. Zhao, Z. Guo, M. Zhang, S. Yang, Lei. Zhao, Surface-interface analysis of In x Ga 1-x As/InP heterostructure in positive and negative mismatch system, Surf. Interface Anal. 51 (5) (2019) 498–505.

[7] B. Smiri, M. Ben Arbia, D. Ilkay, F. Saidi, Z. Othmen, B. Dkhil, A. Ismail, E. Sezai, F. Hassen, H. Maaref, Optical and structural properties of In-rich In $_x$ Ga $_{1-x}$ As epitaxial layers on (1 0 0) InP for SWIR detectors, Mater. Sci. Eng., B 262 (2020) 114769, https://doi.org/10.1016/j.mseb.2020.114769.

[8] T. Asar, S. Özçelik, E. Özbay, Structural and electrical characterizations of In x Ga 1-x As/InP structures for infrared photodetector applications, J. Appl. Phys. 115 (10) (2014) 104502, https://doi.org/10.1063/1.4868056.

[9] J.A. del Alamo, Nanometre-scale electronics with III–V compound semiconductors, Nature 479 (7373) (2011) 317–323.

[10] B. Smiri, T. Hidouri, F. Saidi, H. Maaref, Carriers' localization and thermal redistribution in InAlAs/InP grown by MOCVD on (311)A- and (311)B-InP substrates, Appl. Phys. A 125 (2) (2019), https://doi.org/10.1007/s00339-019-2444-9.

[11] W. Bao, Z. Su, C. Zheng, J. Ning, S. Xu, Carrier Localization Effects in InGaN/GaN Multiple-Quantum-Wells LED Nanowires: Luminescence Quantum Efficiency Improvement and "Negative" Thermal Activation Energy, Sci. Rep. 6 (1) (2016), https://doi.org/10.1038/srep34545.

[12] B. Du, Y.i. Gu, X.-Y. Chen, Y.-J. Ma, Y.-H. Shi, J. Zhang, Y.-G. Zhang, Improved performance of high indium InGaAs photodetectors with InAlAs barrier, Jpn. J. Appl. Phys. 57 (6) (2018) 060302, https://doi.org/10.7567/JJAP.57.060302.

[13] B. Smiri, I. Fraj, F. Saidi, R. Mghaieth, H. Maaref, Effect of piezoelectric field on type II transition in InAlAs/InP (311) alloys with different substrate polarity, J. Alloy. Compd. 736 (2018) 29–34.

[14] B. Smiri, F. Saidi, A. Mlayah, H. Maaref, Power- and temperature-dependent photoluminescence investigation of carrier localization at inverted interface transitions in InAlAs/InP structures, Jpn. J. Appl. Phys. 59 (2) (2020) 022001, https://doi.org/10.7567/1347-4065/ab65a6.

[15] Y.P. Varshni, Temperature dependence of the energy gap in semiconductors, Physica 34 (1) (1967) 149–154.

[16] L. Viña, S. Logothetidis, M. Cardona, Temperature dependence of the dielectric function of germanium, Phys. Rev. B 30 (4) (1984) 1979–1991.

[17] R. Pässler, Basic Model Relations for Temperature Dependencies of Fundamental Energy Gaps in Semiconductors, Phys. Status Solidi B 200 (1) (1997) 155–172, https://doi.org/10.1002/1521-3951(199703)200:1<155::AID-PSSB155>3.0.CO;2-3.

[18] R. Deki, T. Sasaki, M. Takahasi, Strain relaxation and compositional separation during growth of InGaAs/GaAs(001), J. Cryst. Growth 468 (2017) 241–244.

[19] G.P. Dimitrakopulos, C. Bazioti, J. Grym, P. Gladkov, E. Hulicius, J. Pangrác, O. Pacherová, P.h. Komninou, Misfit dislocation reduction in InGaAs epilayers grown on porous GaAs substrates, Appl. Surf. Sci. 306 (2014) 89–93.

[20] J. P. Estrera, W. M. Duncan, Y. C. Kao, H. Y. Liu, P. D. Stevens, et E. A. Beam III, « Systematic optical study of In $_x$ Ga $_{1-x}$ As on InP using photoluminescence, photoreflectance, and micro-Raman spectroscopy », Somerset, NJ, juill. 1992, p. 120, doi: 10.1117/12.60447.

[21] C.-C. Chang, M.-S. Hsu, Y. Ouyang, et Y.-C. Wang, « Optical properties of the modulation doped InGaAs/InAlAs quantum well », in *Photonic Fiber and Crystal Devices: Advances in Materials and Innovations in Device Applications III*, août 2009, vol. 7420, p. 74200S, doi: 10.1117/12.825660.

[22] R. Nedzinskas, B. Čechavičius, J. Kavaliauskas, V. Karpus, G. Valušis, L. Li, S. P. Khanna, E.H. Linfield, Polarized photoreflectance and photoluminescence spectroscopy of InGaAs/GaAs quantum rods grown with As2 and As4 sources, Nanoscale Res. Lett. 7 (1) (2012), https://doi.org/10.1186/1556-276X-7-609.

[23] N. Tounsi, M. M. Habchi, Z. Chine, A. Rebey, et B. El Jani, « Optical properties study of In $_{0.08}$ Ga $_{0.92}$ As/GaAs using spectral reflectance, photoreflectance and near-infrared Photoluminescence », *Superlattices Microstruct.*, vol. 59, p. 133–143, juill. 2013, doi: 10.1016/j.spmi.2013.04.009.

[24] X. Chen, K. Wang, M.C. Beard, Ultrafast probes at the interfaces of solar energy conversion materials, PCCP 21 (30) (2019) 16399–16407.

[25] D.E. Aspnes, A.A. Studna, Schottky-Barrier Electroreflectance: Application to GaAs, Phys. Rev. B 7 (10) (1973) 4605–4625.

[26] B. Smiri, I. Fraj, M. Bouzidi, F. Saidi, A. Rebey, et H. Maaref, « Effect of V/III ratio on the optical properties of (3 1 1)A and (3 1 1) B oriented InAlAs/InP heterostructures », *Results Phys.*, vol. 12, p. 2175–2182, mars 2019, doi: 10.1016/j.rinp.2019.02.035.

[27] D. Yan, F.H. Pollak, V.T. Boccio, C.L. Lin, P.D. Kirchner, J.M. Woodall, R.C. Gee, P. M. Asbeck, Photoreflectance characterization of an InP/InGaAs heterojunction bipolar transistor structure, Appl. Phys. Lett. 61 (17) (1992) 2066–2068.

[28] C.-H. Ho, K.-W. Huang, Y.-S. Lin, et D.-Y. Lin, « Practical photoluminescence and photoreflectance spectroscopic system for optical characterization of semiconductor devices », *Opt. Express*, vol. 13, n° 11, p. 3951–3960, mai 2005, doi: 10.1364/OPEX.13.003951.

[29] W. Zhou *et al.*, « Photoreflectance Characterization of the Semi-Insulating InP Substrate Interface with InGaAs and InAlAs Epilayers », *MRS Proc.*, vol. 281, janv. 2011, doi: 10.1557/PROC-281-121.

[30] B. Tongbram, S. Sengupta, S. Chakrabarti, Impact of an In x Ga $_{1-x}$ As Capping Layer in Impeding Indium Desorption from Vertically Coupled InAs/GaAs Quantum Dot Interfaces, ACS Appl. Nano Mater. 1 (8) (2018) 4317–4331.

[31] I. Fraj, T. Hidouri, F. Saidi, H. Maaref, Carrier localization in In $_{0.21}$ Ga $_{0.79}$ As/GaAs multiple quantum wells: A modified Pässler model for the S-shaped temperature dependence of photoluminescence energy, Superlattices Microstruct. 102 (2017) 351–358.

[32] Q. Li, S.J. Xu, M.H. Xie, S.Y. Tong, A model for steady-state luminescence of localized-state ensemble, Europhys. Lett. 71 (6) (2005) 994–1000.

[33] Z. Su, S. Xu, A generalized model for time-resolved luminescence of localized carriers and applications: Dispersive thermodynamics of localized carriers, Sci. Rep. 7 (1) (2017), https://doi.org/10.1038/s41598-017-00065-3.

[34] Q. Li, S.J. Xu, W.C. Cheng, M.H. Xie, S.Y. Tong, C.M. Che, H. Yang, Thermal redistribution of localized excitons and its effect on the luminescence band in InGaN ternary alloys, Appl. Phys. Lett. 79 (12) (2001) 1810–1812.

[35] Z.C. Su, S.J. Xu, R.X. Wang, J.Q. Ning, J.R. Dong, S.L. Lu, H. Yang, Electroluminescence probe of internal processes of carriers in GaInP single junction solar cell, Sol. Energy Mater. Sol. Cells 168 (2017) 201–206.

[36] H. Wang, Y.i. Gu, C. Yu, S. Zhu, Y. Zhu, P. Chen, J. Cao, Bo. Yang, T. Li, X. Shao, X. Li, H. Gong, Direct correlation of defects and dark currents of InGaAs/ InP photodetectors, Mat. Sci. Semicon. Proc. 123 (2021) 105540, https://doi.org/10.1016/j.mssp.2020.105540.

[37] M.YuI, et al., «Interdot carrier transfer in asymmetric bilayer InAs/GaAs quantum dot structures»., Appl. Phys. Lett. vol.86, no 6, p. 063102, mars 2005, doi: 10.1063/1.1861980.

[38] R.K. Ahrenkiel, R. Ellingson, S. Johnston, M. Wanlass, Recombination lifetime of In0.53Ga0.47As as a function of doping density, Appl. Phys. Lett. 72 (26) (1998) 3470–3472.

[39] B. Deveaud, F. Clérot, N. Roy, K. Satzke, B. Sermage, D. Katzer, Enhanced radiative recombination of free excitons in GaAs quantum wells, Phys. Rev. Lett. 67 (17) (1991) 2355–2358.

[40] I. Fraj, F. Saidi, Z. Zaaboub, L. Bouzaîene, L. Sfaxi, H. Maaref, Optical investigation of In0.21Ga0.79As multiple quantum wells grown on (001) and (113) A GaAs substrates, Superlattices Microstruct. 82 (2015) 406–414.

[41] Y. Shi, L.C. Kreuzer, N.C. Gerhardt, M. Pantouvaki, J. Van Campenhout, M. Baryshnikova, R. Langer, D. Van Thourhout, B. Kunert, Time-Resolved Photoluminescence Characterization of InGaAs/GaAs Nano-Ridges Monolithically Grown on 300 mm Si Substrates, J. Appl. Phys. 127 (10) (2020) 103104, https://doi.org/10.1063/1.5139636.